





Article

The complex mechanism of Ti⁴⁺ incorporation into litidionite from the Somma–Vesuvius volcano, Italy

Giuseppina Balassone^{1,2}, Taras L. Panikorovskii^{3,4*} , Annamaria Pellino¹, Ayya V. Bazai³, Vladimir N. Bocharov⁵ , Sergey V. Krivovichev^{3,4}, Carmela Petti⁶, Piergiulio Cappelletti^{1,6} and Nicola Mondillo^{1,7}

¹Department of Earth Science, Environment and Resources (DiSTAR), University of Naples Federico II, Via Cintia, 26, Naples I-80126, Italy; ²National Institute of Geophysics and Volcanology (INGV), Vesuvius Observatory, Via Diocleziano I-80124 Naples, Italy; ³Kola Science Centre, Russian Academy of Sciences, 14 Fersman Street, Aptity 184200, Russia; ⁴Department of Crystallography, St. Petersburg State University, 7–9 Universitetskaya, Naberezhnaya, St. Petersburg 199034, Russia; ⁵Geo Environmental Centre “Geomodel”, Saint-Petersburg State University, Ul’yanovskaya Str. 1, St. Petersburg 198504, Russia; ⁶Mineralogical Museum, Centre of Natural Sciences Museums, University of Naples Federico II, Via Mezzocannone 8, Naples I-80134, Italy; and ⁷Department of Earth Sciences, Natural History Museum, London, UK

Abstract

For this study, the rare Cu-bearing silicate fumarolic assemblages from the Somma–Vesuvius volcano, Italy, characterised by the rare mineral litidionite, CuKNaSi₄O₁₀, were investigated. We report new data about Cu- and Ti-bearing phases found in these mineralisations, in which Ti-bearing litidionite occurs together with kamenevite, perovskite and rutile. Ti-bearing litidionite appears on the latest stages of partial crystallisation of Ti-bearing silica glass. Incorporation of Ti⁴⁺ into the litidionite crystal structure was investigated in detail. The Raman spectra of Ti-bearing litidionite contains an intense band at 597 cm⁻¹ related to anti-symmetric bending vibrations of Si–O bonds or overlapping stretching vibrations of Ti–O bonds. The bands in the range 350–500 cm⁻¹ correspond to symmetric bending vibrations of O–Si–O bonds and overlapping stretching vibrations of Ti–O bonds. The crystal structure of Ti-litidionite has been refined in the *P* $\bar{1}$ space group, *a* = 6.9699(7), *b* = 7.9953(10), *c* = 9.8227(10) Å, α = 105.186(9), β = 99.458(8) and γ = 114.489(10) to *R*₁ = 0.064 for 1726 unique observed reflections. The refinement of the site-occupation factors confirmed the presence of Ti at a five-coordinated *M* site. The mean bond distance of 2.125 Å for the *M* site agrees with its refined occupancy (Ti_{0.32}Cu_{0.30}Ca_{0.29}Fe_{0.09})_{1.00}. The incorporation of Ti into the litidionite structure is accompanied by the complex heteropolyhedral substitution according to the scheme ^VTi⁴⁺ + ^{VII–VIII}□ + ^{IV}Al³⁺ ↔ ^VCu²⁺ + ^{VII–VIII}(Na,K)⁺ + ^{IV}Si⁴⁺. Two possible configurations for the phase with maximal TiO₂ content (12.06 wt.% or 0.56 Ti apfu) CuTiK□Na₂Si₇AlO₂₀ (*Z* = 1) or CuTiK₂Na□Si₇AlO₂₀ (*Z* = 1) have been proposed.

Keywords: Ti-litidionite, Somma–Vesuvius, Ti incorporation, crystal structure

(Received 30 October 2021; accepted 1 January 2022; Accepted Manuscript published online: 16 February 2022; Associate Editor: G. Diego Gatta)

Introduction

Litidionite is a rare Cu–Na–K-bearing silicate, first discovered at the Somma–Vesuvius volcano, Italy (Scacchi, 1880). At present, the litidionite group contains four minerals: litidionite, CuKNaSi₄O₁₀ (Pozas *et al.*, 1975), manaksite, MnKNaSi₄O₁₀ (Khomyakov *et al.*, 1992), fenaksite, Fe²⁺KNaSi₄O₁₀ (Rozhdestvenskaya *et al.*, 2004) and calcinaksite, CaKNaSi₄O₁₀·H₂O (Chukanov *et al.*, 2015). The litidionite-bearing assemblage is typical of high-temperature alteration processes at the rock-fumaroles interface (Pozas *et al.*, 1975; Balassone *et al.*, 2019). Synthetic analogues of litidionite, manaksite and fenaksite have been obtained under hydrothermal conditions and 230°C (Brandão *et al.*, 2009). Recently, Chukanov *et al.* (2015) described an H₂O-bearing litidionite member calcinaksite. Calcinaksite was first detected in a calcic xenolith hosted by an alkaline basalt at

Bellerberg volcano, Eifel, Germany, as the product of contact metamorphism formed during the high-temperature hydrothermal stage (Aksenov *et al.*, 2014; Chukanov *et al.*, 2015). The second worldwide occurrence of this mineral was recorded at Somma–Vesuvius by Balassone *et al.* (2019). Ti-bearing litidionite associations at Somma–Vesuvius are typically found in deep-blue glassy crusts and are characterised by very unusual thermally modified pyroclastic fragments related to the old fumarolic activity from the 1872 eruption (Scacchi, 1880, 1881; Zamboni, 1910, 1935; Pozas *et al.*, 1975). A re-examination of this type of sample (currently under study) was carried out by Balassone *et al.* (2019).

Litidionite-group minerals are of interest for their magnetic properties. Different electronic configurations and distortion of [M₂²⁺O₈] dimers produce antiferromagnetic interactions within the Mn (manaksite) and Cu (litidionite) dimers, whereas for Fe (fenaksite) dimers ferromagnetic interaction is observed (Brandão *et al.*, 2009).

In this contribution, the occurrence of a relatively low-temperature Ti-bearing litidionite from Somma–Vesuvius from a peculiar association at Somma–Vesuvius is reported. The

*Author for correspondence: Taras L. Panikorovskii, Email: t.panikorovskii@ksc.ru

Cite this article: Balassone G., Panikorovskii T.L., Pellino A., Bazai A.V., Bocharov V.N., Krivovichev S.V., Petti C., Cappelletti P. and Mondillo N. (2022) The complex mechanism of Ti⁴⁺ incorporation into litidionite from the Somma–Vesuvius volcano, Italy. *Mineralogical Magazine* 86, 222–233. <https://doi.org/10.1180/mgm.2022.1>

complex method of incorporation of Ti into the litidionite structure and polyhedral and heteropolyhedral substitutions in the litidionite-group minerals are also discussed.

Volcanological and mineralogical overview

Located in southern Italy, near Naples, the Somma–Vesuvius edifice is a moderately sized (1281 m a.s.l.) stratovolcano consisting of an older edifice dissected by a summit caldera (Somma) and a recent cone (Vesuvius), which grew within the caldera after the 79 AD Pompeii eruption. It belongs to the so-called Neapolitan district, the southernmost cluster of volcanoes of the Roman Magmatic Province (RMP, central-southern Italy), which is related genetically to the alkaline–potassic magmatism in the Central Mediterranean, developed from Oligocene to present as a result of the convergence of Africa and Eurasia.

The Somma caldera is a nested, poly-phased structure formed by several collapses related to the main explosive eruptions (Cioni *et al.*, 1999, 2008). It consists of a pile of thin lava flows interbedded with spatter and cinder deposits post-dating the 39 ka old Campanian Ignimbrite of Campi Flegrei (Avanzinelli *et al.*, 2017, and references therein). The formation of the Somma caldera was completed with the famous AD 79 Pompeii Plinian eruption, afterwards the Vesuvius cone began to form discontinuously during periods of open conduit activity that occurred in the 1st–3rd centuries, 5th–8th, 9th centuries, 10th–11th centuries and in 1631–1944 AD.

The most recent period (1631–1944 AD) was characterised by summit or lateral lava effusions and semi-persistent, mild explosive activity (small lava fountains, gases and vapour emission from the crater) interrupted by pauses lasting from months to a maximum of seven years (Di Renzo *et al.*, 2007; Avanzinelli *et al.*, 2017, and references therein). Since the last eruption of 1944, Vesuvius is quiescent (closed-conduit phase), as it has not shown signs of unrest and only moderate seismicity and fumaroles testify its activity (Avanzinelli *et al.*, 2017, and references therein).

At Somma–Vesuvius the magmatic products mainly display a potassic to ultrapotassic character and the copper-bearing mineralisation are related mainly to the most recent eruptive period of 1631–1944 AD, when strong fumarolic events occurred. Diffuse exhalative mineralisation took place, with a great variety of mineral species. With regard to the Cu-bearing phases, highly variable mixtures of sulfates, halides, oxides, vanadates and sulfides are observed (see Balassone *et al.*, 2019 for further details).

At Vesuvius, a strong eruption occurred in April 1872, produced by strombolian activity with a lava fountain (3 days for the main phase) and ejection of scoria, lapilli, ash and mud flows (Arrighi *et al.*, 2001). In June 1873, a mineral collector at the Vesuvius crater found small lapilli covered by deep-blue crusts typically with a peculiar glassy to enamelled-like appearance and brought them to the Neapolitan mineralogist Eugenio Scacchi. He characterised the blue material as a new mineral species – a copper, sodium and potassium silicate – and named it litidionite after ‘λιτιδιον’, the Greek word for lapilli (Scacchi, 1880). Then, Arcangelo Scacchi, the father of Eugenio and director of the Mineralogical Museum of Naples, analysed some scoriae covered by blue–white sublimate products found in October 1880 at the Vesuvian crater, and established that the blue material was a new copper mineral, that he called ‘neocyanite’, whereas the white part was described as ‘opal’. Afterwards, Zambonini

(1910, 1935) determined the relationship between litidionite and ‘neocyanite’.

This rare silicate has been recorded in only two other occurrences: in fumarolic sublimates of the Tolbachik volcano, Kamchatka, Russia (Shchipalkina *et al.*, 2019, 2020b) and at Pyro Pit Snowstorm mine (Mountain View mine), Nevada, USA (Castor and Ferdock, 2003; <https://www.mindat.org/min-2422.html>).

According to Balić-Žunić *et al.* (2016), minerals found in European fumaroles are impressive due to the number of different species found, especially taking into account the fact that some prolific mineral groups, e.g. silicates and phosphates, do not contribute to the species list or contribute very little. Among the European fumarole localities, Vesuvius and Vulcano island in Italy show the richest mineralogy; as concerns Vesuvius, this status is due to the exceptional abundance of otherwise rare elements in its emanations, such as Cu, Cr, Mn, Ni, B, Tl, Pb, As and Se (Balić-Žunić *et al.*, 2016).

As regards the silicate occurrences in the fumarolic environments, Shchipalkina *et al.* (2020b) also observed that the silicate-bearing associations are rare, and the main minerals in most of fumaroles related to active volcanoes are sulfates, halides, oxides and sulfides. A thorough investigation on silicate-bearing mineralisation in sublimates in active volcanic fumaroles related to the Tolbachik volcano in Kamchatka, Russia was carried out by Shchipalkina *et al.* (2019, 2020a, 2020b, 2020c). These authors reported that fumarolic silicates in the Tolbachik volcano are typically enriched with ‘ore’ elements, i.e. Cu, Zn, Sn, Mo, W and As (Shchipalkina *et al.*, 2020b), virtually hydrogen-free, and formed in the temperature range 500–800°C as a result of direct deposition from the gas phase (as volcanic sublimates) or gas–rock interactions.

Even though our survey on the Cu-bearing silicates and associated minerals from the 1872 eruption of Vesuvius is still in progress, similarities between the Tolbachik and Vesuvius occurrences in terms of silicate mineral assemblages can be pointed out. For example, Balassone *et al.* (2004) found rare silicate (+oxides, sulfates, etc.)-bearing assemblages (with fluorophlogopite, indialite, magnetite, hematite and gypsum) in some 1872 AD ejected breccia that had been strongly hydrothermally modified at high temperatures, which is similar to some mineral assemblages (with fluorophlogopite, indialite, copper-rich oxide spinels, hematite, anglesite and baryte) recorded at the Tolbachik volcano by Pekov *et al.* (2018).

According to our data (see also Balassone *et al.*, 2019), litidionite from Somma–Vesuvius has an extremely complex association of different silicates, basically consisting of litidionite, calcinaksite, tridymite, wollastonite, diopside and a glassy phase. Various traces of non-silicates are also recorded (see Results section), and it is very likely that further minor to trace phases will be identified in this Vesuvian mineral assemblage from our ongoing research on new sample sets.

Materials and methods

The litidionite-bearing samples, #17926 E6457 and 161 c.v. (Fig. 1), are from the Mineralogical Museum of the University of Naples Federico II (Italy) and belong to the vast collection devoted to the Somma–Vesuvius volcano. Preliminary investigations on sample #17926 E6457 were previously carried out by Balassone *et al.* (2019), whereas sample #161 c.v. is part of a new set of litidionite-bearing samples currently under investigation. Samples with copper-bearing minerals represent a



Fig. 1. The Ti-litidionite-bearing samples studied. (a) Sample 17926 E6457: the fragment on the left side shows small lapilli with a tiny blue litidionite-rich crust between them, whereas the fragment on the right side represents typical encrustations of litidionite and associated neoformed minerals. (b) Sample 161 c.v.: the fragment on the left side is made mainly of mixed amorphous silicate material and litidionite, the fragment on the right side is composed of litidionite (blue part) and a mixture of tridymite, diopside, kamenevite and glass (white part). The length of the Museum labels is 7 cm.

significant part of the Vesuvian collection and typically occur as encrustations and/or tiny patinas, coatings and/or void filling associated with the historical activity of Vesuvius (Balassone *et al.*, 2019). Litidionite and the associated minerals are found in shiny deep-blue to white crusts, sometimes with a glassy aspect, on lava fragments or small lapilli affected severely by the fumarolic activity (Balassone *et al.*, 2019, and references therein).

Back-scattered electron (BSE) images of sample #17926 E6457 were carried out using a LEO-1450 scanning electron microscope (SEM) with a Quantax 200 energy-dispersive spectrometer (EDS). The chemical composition was determined with the Cameca MS-46 electron microprobe (Geological Institute of the Kola Science Center, Russian Academy of Sciences) operating in a wavelength-dispersive mode (WDS) at 20 kV and 20–30 nA. The electron beam diameter used was 1–10 μm . The following standards were used: lorenzenite (Na and Ti); pyrope (Mg and Al); diopside (Si and Ca); wadeite (K); hematite (Fe); metallic niobium (Nb); metallic copper (Cu); wulfenite (Pb) and atacamite (Cl).

Imaging and analysis of sample #161 c.v. were carried out using a Jeol JSM5310 scanning electron microscope with an

Oxford EDS equipped with an INCA X-stream pulse processor and the 4.08 version *Inca* software (Department of Earth Science, Environment and Resources, DiSTAR, University of Naples Federico II Italy). The operating conditions were an acceleration voltage of 15 kV, 50–100 μA filament current, variable spot size and a working distance of 20 mm; the reference standards used for quantitative microanalysis were: anorthoclase (Si, Al and Na); diopside (Ca); microcline (K); rutile (Ti); fayalite (Fe); olivine (Mg); serandite (Mn); sphalerite (Zn); benitoite (Ba); celestite (Sr); fluorite (F); halite (Cl); pyrite (S); galena (Pb); and pure metal (Cu). Detection limits of the elements analysed are <0.1%. Composition of litidionites from sample #161 c.v. was also determined with a Cameca SX50 WDS (Institute of Environmental Geology and Geoenvironment, National Research Council, IGAG CNR, Rome). Operating conditions were 15 kV acceleration voltage, 15 nA beam current and 10 mm spot size. Oxides, silicates and pure metals were used as standards. Raw elemental data were corrected using the *PAP* programs (Pouchou and Pichou, 1991).

Cation contents were calculated with the *MINAL* program of D. Dolivo-Dobrovolsky (Dolivo-Dobrovolsky, 2016).

Statistical analyses were carried out with *STATISTICA 8.0* (StatSoft. Inc., 2008).

Raman spectra of Ti-bearing litidionite sample #17926 E6457, collected from uncoated polished sections, were recorded with a Horiba Jobin-Yvon LabRAM HR800 spectrometer equipped with an Olympus BX-41 microscope in back-scattered geometry. Raman spectra were excited by a He-Ne laser (632.8 nm) with actual power of 2 mW under the 50× objective with a numerical aperture equal to 0.75. The spectra were obtained in the range of 70–4000 cm^{-1} at a resolution of 2 cm^{-1} at room temperature with a 2 μm beam diameter and 150 s acquisition time. The spectra were processed using *Labspec* (Jobin Yvon) and *Origin* software (OriginLab Corporation, Northampton, MA, USA).

The crystal-structure studies on sample #17926 E6457 were carried out at the X-ray Diffraction Resource Centre of

St. Petersburg State University by means of the Rigaku XtaLAB Supernova diffractometer equipped with CCD detectors using monochromatic $\text{CuK}\alpha$ radiation ($\lambda = 1.54184 \text{ \AA}$) at room temperature. More than a half sphere of the diffraction sphere was collected (scanning step 1° and exposure time 10–40 s). The data were integrated and corrected using the Rigaku *CrysAlisPro* program package, which was also used to apply an empirical absorption correction using spherical harmonics, as implemented in the *SCALE3 ABSPACK* scaling algorithm (Agilent Technologies, 2014). The crystal structure of Ti-bearing litidionite was refined to $R_1 = 0.063$ ($R_{\text{int}} = 0.041$) for 1730 independent reflections with $F_o > 4\sigma(F_o)$ in $P\bar{1}$ space group using the *SHELXL* software package (Sheldrick, 2015). The crystal structure was drawn using the *VESTA 3* program (Momma and Izumi, 2011). The distortion indexes for

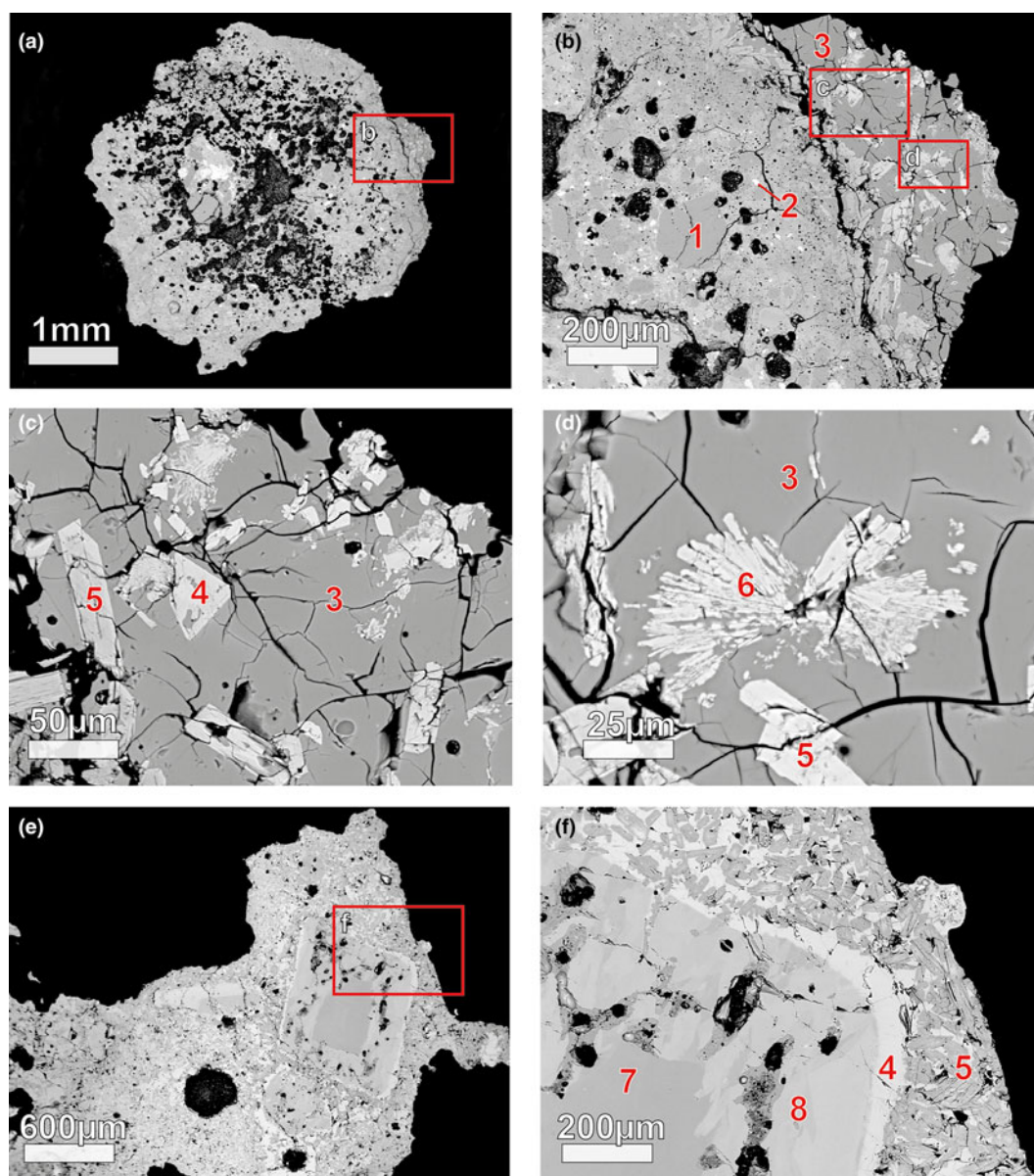


Fig. 2. BSE image of litidionite-group minerals in the lapilli from Somma-Vesuvius, sample #17926 E6457: 1 – Al-bearing diopside, 2 – perovskite, 3 – Si-glass, 4 – litidionite, 5 – calclnaksite, 6 – kamenevite, 7 – diopside and 8 – Fe-bearing diopside.

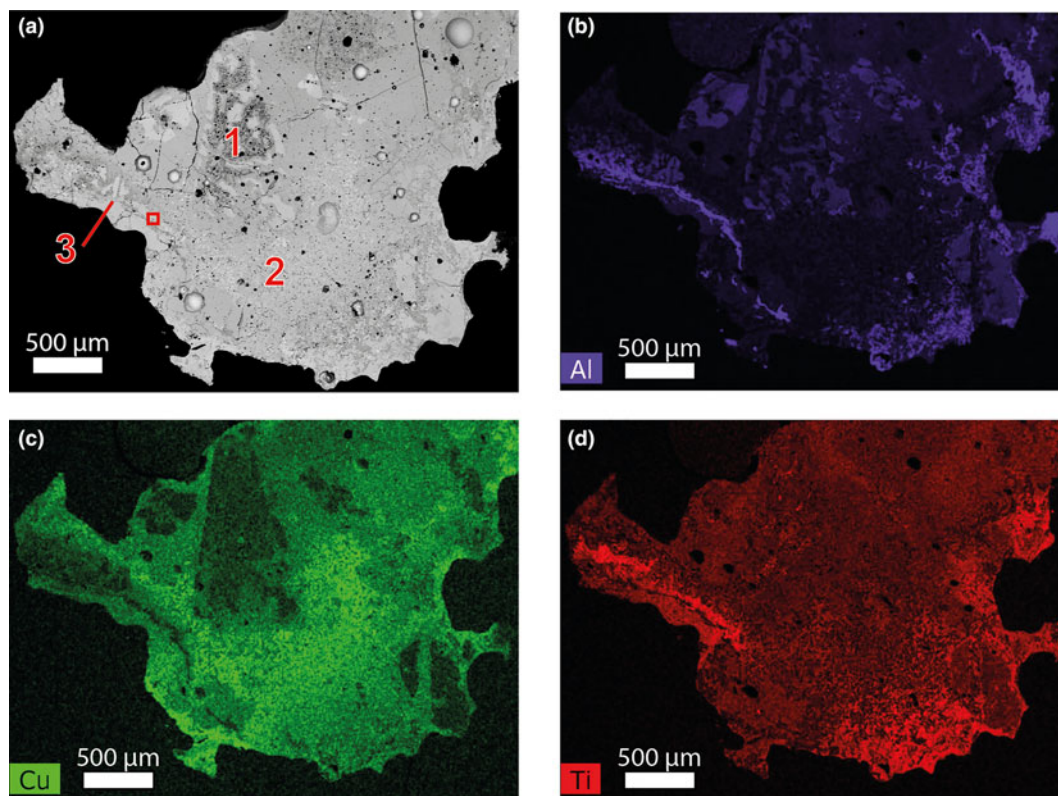


Fig. 3. (a) BSE image of Ti-bearing litidionite areas, sample #17926 E6457: 1 - Fe-bearing diopside, 2 - litidionite and 3 - Ti-bearing litidionite; (b,c,d) X-ray distribution maps for Al K, Cu K and Ti K α radiation. The area studied by Raman spectroscopy is indicated by a red square.

Table 1. Elemental composition (wt. %) and coefficients in the formula (atoms per formula unit, on the basis on Al + Si = 4 apfu) of litidionite-group minerals from the Somma-Vesuvius complex, sample #17926 E6457 (analyses 1–5) and sample #161 c.v. (analyses 6–10), obtained by WDS analyses.

Wt.%	1	2	3	4	5	6	7	8	9	10
SiO ₂	60.80	63.73	66.41	64.45	61.23	59.07	68.4	62.18	61.76	58.11
Al ₂ O ₃	3.57	3.69	3.49	3.22	2.91	0.26	0.86	0.17	0.25	3.06
TiO ₂	9.65	4.54	2.75	4.45	12.06	0.21	1.22	0.02	0.37	3.85
FeO	1.53	1.05	0.92	0.79	1.08	–	0.29	0.06	–	1.24
MnO	–	–	–	–	–	–	0.20	0.24	–	–
MgO	3.25	3.23	3.09	3.86	3.16	0.28	0.40	0.38	0.56	3.44
CaO	1.88	2.03	2.37	2.36	1.55	0.88	0.86	11.48	11.67	3.40
CuO	2.25	2.66	3.35	3.50	2.29	19.72	6.61	5.47	3.93	4.46
Na ₂ O	5.22	7.20	7.39	6.17	4.82	9.2	7.34	9.75	9.35	9.91
K ₂ O	10.52	10.38	10.08	10.09	9.95	10.22	7.71	11.12	10.99	10.25
PbO	0.25	0.42	0.42	0.34	0.44	0.16	4.27	–	–	0.82
Cl	0.60	–	0.13	0.21	0.37	–	–	0.10	–	0.72
–O = Cl ₂	0.14	–	0.03	0.05	0.08	–	–	0.02	–	0.16
Total	99.93	98.93	100.35	99.36	99.78	100.00	98.16	100.95	98.88	99.10
Apfu										
Si ⁴⁺	3.74	3.74	3.77	3.78	3.79	3.98	3.94	3.99	3.98	3.77
Al ³⁺	0.26	0.26	0.23	0.22	0.21	0.02	0.06	0.01	0.02	0.23
Ti ⁴⁺	0.45	0.20	0.12	0.20	0.56	0.01	0.05	0.00	0.02	0.19
Fe ²⁺	0.08	0.05	0.04	0.04	0.06	0.00	0.01	0.00	0.00	0.07
Mn ²⁺	0.00	0.00	0.00	0.00	0.00	0.00	0.01	0.01	0.00	0.00
Mg ²⁺	0.30	0.28	0.26	0.34	0.29	0.03	0.03	0.04	0.05	0.33
Ca ²⁺	0.12	0.13	0.14	0.15	0.10	0.06	0.05	0.79	0.80	0.24
Cu ²⁺	0.10	0.12	0.14	0.16	0.11	1.00	0.29	0.26	0.19	0.22
Na ⁺	0.62	0.82	0.81	0.70	0.58	1.20	0.82	1.21	1.17	1.25
K ⁺	0.83	0.78	0.73	0.75	0.79	0.88	0.57	0.91	0.90	0.85
Pb ²⁺	0.00	0.01	0.01	0.01	0.01	0.00	0.07	0.00	0.00	0.02
Cl [–]	0.06	0.00	0.01	0.02	0.04	0.00	0.00	0.01	0.00	0.08

‘–’ = not detected

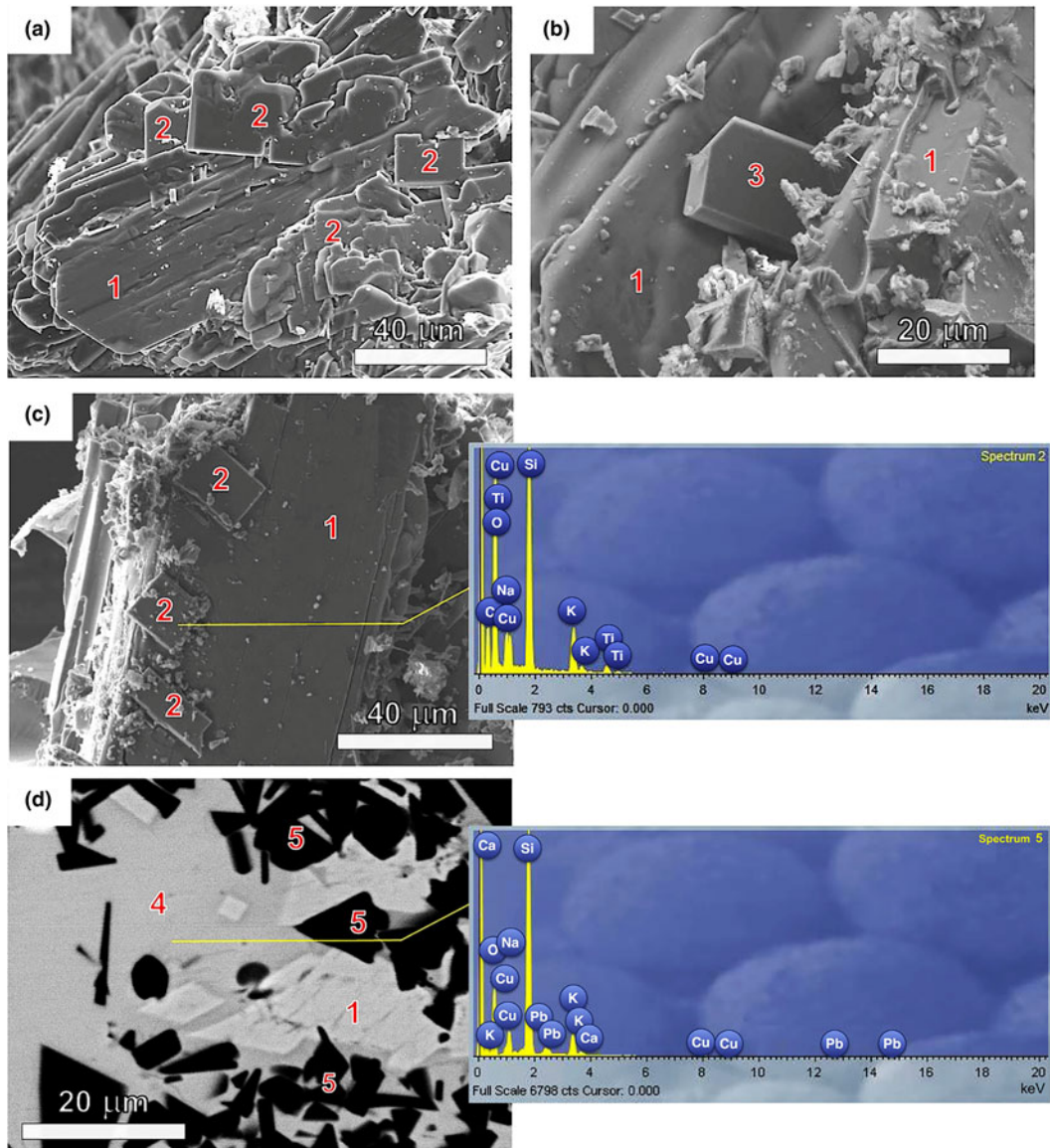


Fig. 4. SEM-BSE images of litidionite varieties in sample #161 c.v.: (a), (b), (c) SEM micrographs of sample fragments; (d) BSE image in polished section. 1 – litidionite, 2 – Ti-bearing litidionite, 3 – kamenevite, 4 – Pb-bearing litidionite and 5 – tridymite.

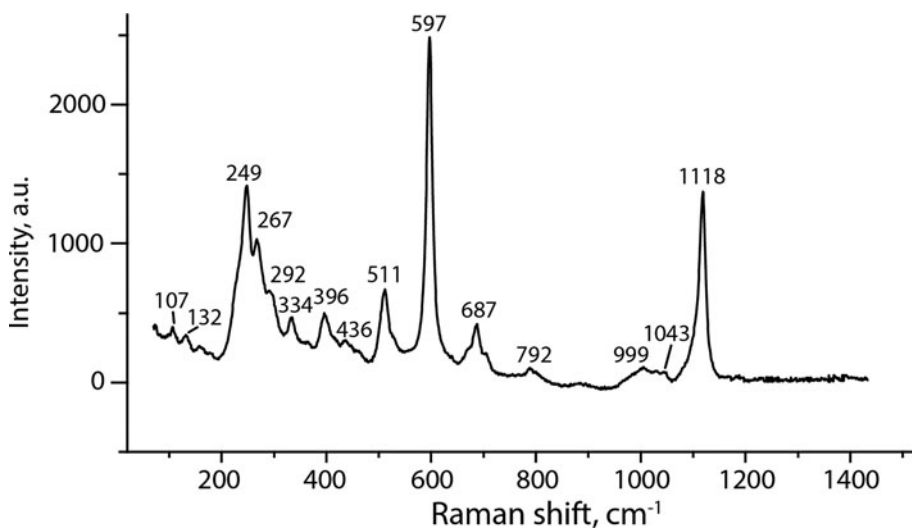


Fig. 5. Raman spectrum of Ti-bearing litidionite, sample #17926 E6457.

Table 2. Crystal data and structure refinement for Ti-bearing litidionite.

Crystal data	
Crystal system	Triclinic
Space group	$P\bar{1}$
a (Å)	6.9699(7)
b (Å)	7.9953(10)
c (Å)	9.8227(10)
α (°)	105.186(9)
β (°)	99.458(8)
γ (°)	114.489(10)
V (Å ³)	456.95(10)
Formula weight	377.38
Z	2
Density (g·cm ⁻³)	2.732
Absorption coefficient (mm ⁻¹)	16.032
Data collection	
X-ray radiation/power	CuK α ($\lambda = 1.54184$)
Temperature (K)	293(2)
Crystal size (mm)	0.17 × 0.11 × 0.07
$F(000)$	370.0
2θ range (°)	9.816 to 140.818
Index ranges	$-8 \leq h \leq 8, -9 \leq k \leq 9, -9 \leq l \leq 11$
Reflections collected	3446
Independent reflections	1726 [$R_{in} = 0.0415, R_{sigma} = 0.0575$]
Data/restraints/parameters	1726/0/154
Weighting scheme	0.1024 2.1758
Reflections with $F_o > 4\sigma(F_o)$	1516
Refinement	
GoF on F^2	1.079
Final R indexes [$I \geq 2\sigma(I)$]	$R_1 = 0.0635, wR_2 = 0.1737$
R indices (all data)	$R_1 = 0.0694, wR_2 = 0.1799$
Largest diff. peak/hole (e ⁻ ·Å ⁻³)	1.34/-1.19

polyhedra were calculated according to the formula proposed by Baur (1974).

Results

Chemical composition

In the analysed sample #17926 E5457 (Figs 2 and 3), there are four different types of litidionite-group minerals which crystallise in the following order: euhedral and platy crystals of litidionite or Ca-bearing litidionite up to calcinaksite (Fig. 2c) → altered zones

around diopside crystals consisting of litidionite (Fig. 2e,f) or fine-grained litidionite (Fig. 3a) → coarse-grained calcinaksite crystals in the litidionite matrix (Fig. 2f) → marginal zones of lapilli represented by Ti-bearing non-stoichiometric litidionite (Fig. 3a).

In this sample, litidionite occurs in two assemblages, i.e. with tridymite, diopside, calcinaksite, wollastonite, minor amorphous silica-rich glass, kamenevite (K₂TiSi₃O₉·H₂O, the second occurrence after Pekov *et al.*, 2019), perovskite, spinel, atacamite, magnetite or with ilmenite, apatite, rutile, kamenevite, perovskite, Fe-Al spinel, atacamite and halite. Table 1 shows the chemical composition of Ti-bearing litidionite. The Ti content in the litidionite reached up to 12.06 wt.% or 0.56 atoms per formula unit (apfu). The Ti-rich zones are Si-, Cu-, K-, Na-deficient and Al-, Mg-, Pb-enriched (Fig. 3a–d). Note the presence of small amounts of Al, as well as traces of Pb and Cl in the chemical composition in Ti-bearing litidionite only.

In sample #161 c.v. (Table 1) we recorded both a litidionite almost similar to the stoichiometric composition, with very low Ti content, and a Ti-bearing phase (up to 3.95 wt.%), even though we have not observed high Ti amounts as in sample #17926 E5457, at least in the analysed areas.

Figure 4 shows SEM-BSE micrographs of litidionite together with Ti-bearing litidionite detected in sample #161 c.v. (Fig. 4a,c). Note that Ti-litidionite is always later than litidionite, as already observed in the previous sample. In Fig. 4d, an unusual composition, which could correspond to a Pb-rich litidionite, was also found. It is worth noting that Zambonini (1935) reported significant amounts of Pb in litidionite. Selected compositional analyses of litidionite, Ti- and Pb-bearing litidionite are presented in Table 1. Mixed litidionite–calcinaksite compositions occur in association with kamenevite (Fig. 4b), REE-bearing perovskite, celestine, glass and an unknown Na–K sulfate.

Chemical compositions of selected minerals associated with litidionite are presented in the Supplementary table S1.

Raman spectroscopy

The spectrum of Ti-bearing litidionite (#17926 E5457) is close to that of reference litidionite from Vesuvius taken from sample R130088 of the RRUFF project (Lafuente *et al.*, 2015). The Raman spectrum (Fig. 5) contains an intense band at

Table 3. Atom coordinates, displacement parameters (Å²) and site occupancy for the structure of Ti-bearing litidionite.

Site	x/a	y/b	z/c	Occupancy*	ssf _{exp} (e ⁻)	ssf _{calc} (e ⁻)	U_{eq}
Ti1	0.6611(2)	0.1227(2)	0.9105(1)	Ti _{0.32} Cu _{0.30} Ca _{0.29} Fe _{0.09}	23.89	23.88	0.0208(4)
Si1	0.3468(3)	0.6195(3)	0.7739(2)	Si _{0.90} Al _{0.10}	13.46	13.90	0.0282(5)
Si2	0.4546(3)	0.2858(2)	0.7109(2)	Si _{0.95} Al _{0.05}	13.74	13.95	0.0215(5)
Si3	0.9293(3)	0.6400(3)	0.7766(2)	Si _{0.90} Al _{0.10}	13.60	13.90	0.0278(5)
Si4	0.3113(3)	0.1782(3)	0.3631(2)	Si _{0.95} Al _{0.05}	13.74	13.95	0.0256(5)
K1	0.8409(2)	0.2036(2)	0.5052(2)	K _{0.91} □ _{0.09}	17.29	17.29	0.0295(4)
Na1	1.1596(4)	1.1264(4)	0.9079(3)	Na _{0.75} □ _{0.25}	8.25	8.25	0.0105(6)
O1	0.4741(8)	0.7966(7)	0.9286(6)	O	8.00	8.00	0.0316(11)
O2	0.3347(10)	0.4109(8)	0.7736(8)	O	8.00	8.00	0.0451(15)
O3	0.4071(8)	0.1114(7)	0.7685(6)	O	8.00	8.00	0.0297(11)
O4	0.7145(8)	0.4380(8)	0.7558(8)	O	8.00	8.00	0.0435(15)
O5	0.3536(14)	0.1885(9)	0.5325(6)	O	8.00	8.00	0.061(2)
O6	1.0466(9)	0.7976(7)	0.9404(6)	O	8.00	8.00	0.0321(11)
O8	0.5477(8)	0.3308(7)	0.3559(6)	O	8.00	8.00	0.0326(11)
O7	1.0897(8)	0.5664(7)	0.7079(6)	O	8.00	8.00	0.0346(12)
O9	0.2115(8)	-0.0388(7)	0.2518(6)	O	8.00	8.00	0.0341(12)
O10	0.1435(8)	0.2674(8)	0.3388(6)	O	8.00	8.00	0.0362(12)

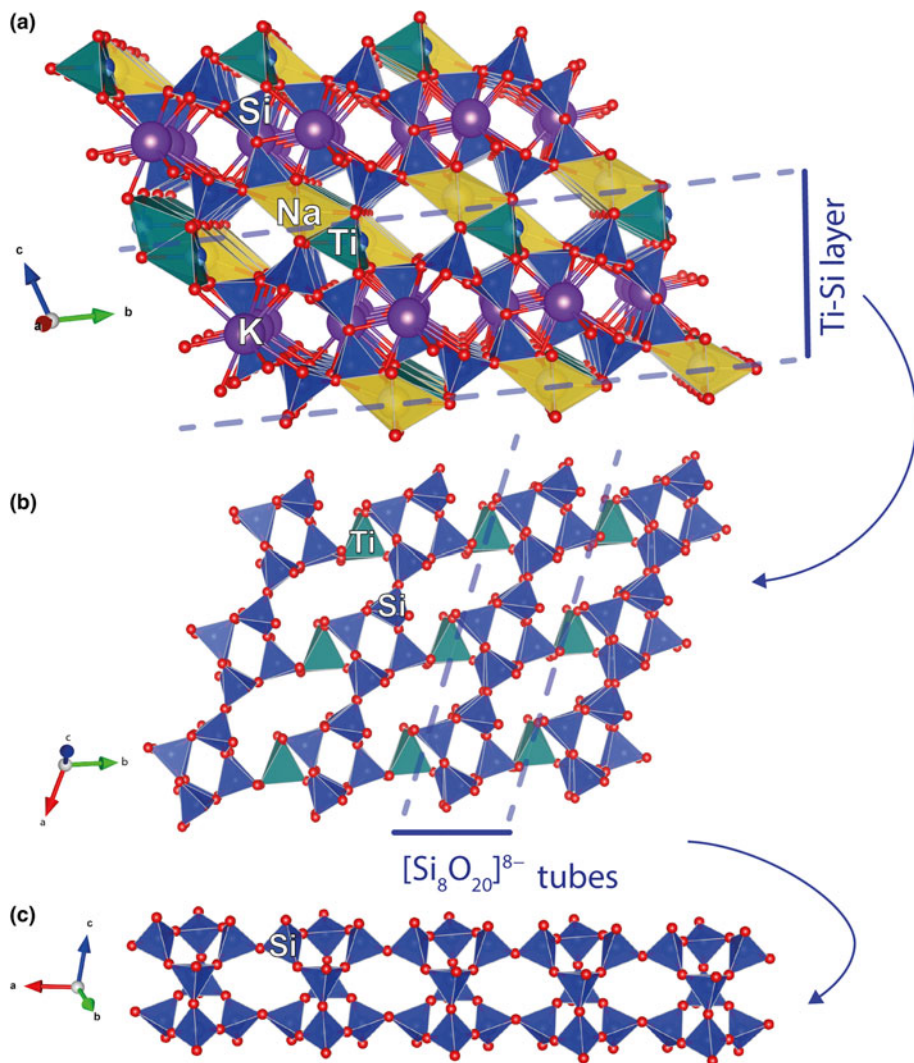
*Occupancies calculated in accordance with the chemical composition and ssf_{exp}, and fixed during refinement.

Table 4. Anisotropic displacement parameters (\AA^2) for the structure of Ti-bearing litidionite.

Site	U^{11}	U^{22}	U^{33}	U^{23}	U^{13}	U^{12}
Ti1	0.0116(5)	0.0218(6)	0.0290(6)	0.0148(5)	0.0044(4)	0.0056(4)
Si1	0.0120(8)	0.0223(9)	0.0467(12)	0.0129(8)	0.0056(8)	0.0062(7)
Si2	0.0133(8)	0.0205(9)	0.0325(10)	0.0170(7)	0.0062(7)	0.0058(7)
Si3	0.0146(9)	0.0237(9)	0.0451(12)	0.0151(8)	0.0098(8)	0.0075(7)
Si4	0.0189(9)	0.0223(9)	0.0320(10)	0.0162(7)	0.0025(7)	0.0050(7)
K1	0.0206(7)	0.0239(7)	0.0391(9)	0.0150(6)	0.0069(6)	0.0050(6)
Na1	0.0041(12)	0.0100(13)	0.0176(14)	0.0104(11)	0.0040(11)	0.0002(10)
O1	0.015(2)	0.028(3)	0.049(3)	0.019(2)	0.005(2)	0.007(2)
O2	0.033(3)	0.034(3)	0.084(5)	0.029(3)	0.035(3)	0.019(3)
O3	0.028(3)	0.022(2)	0.039(3)	0.019(2)	0.011(2)	0.007(2)
O4	0.018(3)	0.032(3)	0.084(4)	0.033(3)	0.011(3)	0.009(2)
O5	0.096(6)	0.032(3)	0.028(3)	0.018(2)	0.002(3)	0.008(3)
O6	0.033(3)	0.029(3)	0.043(3)	0.022(2)	0.017(2)	0.015(2)
O7	0.015(2)	0.030(3)	0.045(3)	0.004(2)	0.004(2)	0.007(2)
O8	0.018(2)	0.027(2)	0.043(3)	0.009(2)	0.004(2)	0.006(2)
O9	0.026(3)	0.025(2)	0.040(3)	0.016(2)	-0.002(2)	0.004(2)
O10	0.024(3)	0.041(3)	0.050(3)	0.021(3)	0.015(2)	0.017(2)

Table 5. Selected bond distances (\AA) in the crystal structure of Ti-bearing litidionite.

Ti1-O6	2.039(5)	Si1-O7	1.629(5)
Ti1-O3	2.019(5)	Si1-O2	1.633(6)
Ti1-O1	2.065(6)	Si1-O8	1.629(6)
Ti1-O9	2.044(6)	Si1-O1	1.578(6)
Ti1-O1	2.456(5)	<Si1-O>	1.617
<Ti1-O>	2.125		
		Si2-O2	1.618(6)
K1-O3	2.806(5)	Si2-O3	1.571(5)
K1-O9	3.017(5)	Si2-O4	1.608(5)
K1-O8	2.980(5)	Si2-O5	1.611(6)
K1-O10	2.839(6)	<Si2-O>	1.602
K1-O7	2.656(5)		
K1-O5	2.740(6)	Si3-O4	1.617(5)
K1-O7	3.100(6)	Si3-O7	1.624(5)
K1-O4	3.164(7)	Si3-O6	1.580(6)
<K1-O>	2.913	Si3-O10	1.628(6)
		<Si3-O>	1.612
Na1-O6	2.369(6)		
Na1-O6	2.537(5)	Si4-O5	1.615(6)
Na1-O3	2.393(6)	Si4-O8	1.620(5)
Na1-O1	2.512(5)	Si4-O9	1.564(5)
Na1-O9	2.496(6)	Si4-O10	1.620(5)
Na1-O10	3.009(6)	<Si4-O>	1.605
Na1-O2	2.865(6)		
<Na1-O>	2.597		

**Fig. 6.** Crystal structure of Ti-bearing litidionite: (a) general view; (b) titanosilicate heteropolyhedral layer; and (c) silicate tubes.

1118 cm^{-1} , which, together with weak bands at 1043 and 999 cm^{-1} , can be assigned to the Si–O–Si and O–Si–O asymmetric stretching vibrations in the $[\text{Si}_8\text{O}_{20}]^{8-}$ groups. The band at 687 and weak band at 792 cm^{-1} are related to the symmetric stretching vibrations of the same bonds (Yakovenchuk et al., 2019). The most intense band at 597 cm^{-1} is related to the asymmetric bending vibrations of Si–O bonds or overlapping stretching vibrations of Ti–O bonds (Filippi et al., 2007; Celestian et al., 2013). The bands in the range 350–500 cm^{-1} correspond to symmetric bending vibrations of O–Si–O bonds and overlapping stretching vibrations of Ti–O bonds (Filippi et al., 2007; Pakhomovsky et al., 2018; Yakovenchuk et al., 2019). The bands at 292 and 334 cm^{-1} are assigned to the symmetric bending vibrations of the Si–O bonds. The strong band at 249 together with 267 cm^{-1} correspond to the bending/stretching vibrations of the Na–O bonds of the NaO_6 coordination polyhedra (Yakovenchuk et al., 2019). The bands below 150 cm^{-1} can be assigned to the lattice vibrations. No boron-bearing groups and water molecules were detected, as the bands in the range of 1150 to 1650 cm^{-1} were absent.

Single-crystal X-ray diffraction

Occupancies of the cation sites were calculated from the experimental site-scattering factors (ssf_{exp}) in accordance with empirical chemical composition. The ssf_{exp} for the Na, Si and K sites was obtained from unconstrained refinement of Si1–4, Na1 and K1 site occupancies. The Ti site was refined initially with occupancy $(\text{Ti}_{0.73}\text{Cu}_{0.27})_{1.00}$ and its resulting occupancy $(\text{Ti}_{0.32}\text{Cu}_{0.30}\text{Ca}_{0.29}\text{Fe}_{0.09})_{1.00}$ is calculated in accordance with the chemical composition and ssf_{exp} and was fixed during refinement. Experimental details are shown in Table 2. The final atomic coordinates and displacement parameters are given in Table 3 and Table 4, selected interatomic distances are in Table 5. The crystallographic information file has been deposited with the Principal Editor of *Mineralogical Magazine* and is available as Supplementary material (see below).

The crystal structure of Ti-bearing litidionite consists of a complex heteropolyhedral pseudolayered framework (Fig. 6a). The Cu–Si pseudolayers (Fig. 6b) are based on the infinite tubes $[\text{Si}_8\text{O}_{20}]^{8-}$ running along [100] (Fig. 6c). The layers are connected by the $[\text{M}_2^{2+}\text{O}_8]$ dimers into a three-dimensional framework (Golovachev et al., 1970; Kornev et al., 1972; Pozas et al., 1975). The cavities in the structure are represented by three types of channels populated by Na^+ and K^+ cations.

The crystal structure contains four symmetrically independent Si tetrahedra with Si–O bond distances in the range 1.564–1.633 Å. According to the refined site-scattering factors (ssf) for Si sites of 13.46, 13.74, 13.60 and 13.74 e^- for Si1, Si2, Si3 and Si4 sites, there is a small admixture of Al in each site. The mean bond lengths for the $\langle\text{Si1–O}\rangle$, $\langle\text{Si2–O}\rangle$, $\langle\text{Si3–O}\rangle$ and $\langle\text{Si4–O}\rangle$ tetrahedra are 1.617, 1.602, 1.612, and 1.605, respectively.

The Na1 site in the litidionite structure is 7-coordinated with a mean $\langle\text{Na–O}\rangle$ distance of 2.597 Å. The refined occupancy of the Na1 site is 0.75, in accordance with ssf of 8.25 e^- . The K is 8-coordinated with the mean $\langle\text{K–O}\rangle$ distance of 2.913 Å. The refined occupancy is 0.91. The chemical analysis demonstrates the deficit of K and Na and we propose that 0.25 of Na1 and 0.09 of K1 sites are vacant.

The square-pyramidal sites form $[\text{Ti}_2\text{O}_8]$ dimers (Fig. 7a) with a Ti–Ti distance of 3.382 Å. In the sample investigated, the five-coordinated site is occupied predominantly by Ti atoms. The

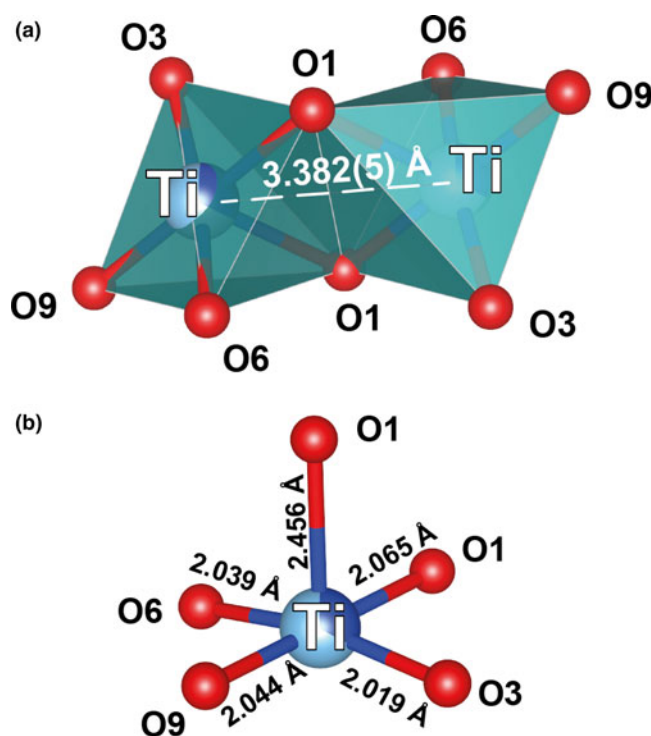


Fig. 7. (a) The M_2O_8 (Ti) dimeric unit and (b) the distortion of bonds in the TiO_5 square pyramid in the crystal structure of Ti-bearing litidionite.

bond lengths are typically distorted for a square pyramid with one long Ti–O bond of 2.456 Å and four shorter bonds in the range 2.019–2.039 Å (Fig. 7b). The distortion index of the TiO_5 square pyramid is 0.061, slightly less than the value of 0.089 observed for litidionite (Brandão et al., 2009) with full occupancy by Cu^{2+} that is in agreement with the decreasing Jahn–Teller distortion associated with the decreasing Cu content. The mean bond distance of 2.125 Å is in good agreement with its refined occupancy $(\text{Ti}_{0.32}\text{Cu}_{0.30}\text{Ca}_{0.29}\text{Fe}_{0.09})_{\Sigma 1.00}$, which in turn agrees with the observed and calculated ssf of 23.89 and 23.88 e^- , respectively.

The final crystal-chemical formula for Ti-bearing litidionite from Somma–Vesuvius can be written as follows: $(\text{K}_{0.91}\square_{0.09})_{\Sigma 1.00}(\text{Na}_{0.75}\square_{0.25})_{\Sigma 1.00}(\text{Ti}_{0.32}\text{Cu}_{0.30}\text{Ca}_{0.29}\text{Fe}_{0.09})_{\Sigma 1.00}(\text{Si}_{3.70}\text{Al}_{0.30})_{\Sigma 4.00}\text{O}_{10}$, where \square = vacancy, which is in good agreement with the chemical analyses and Raman data.

Discussion

In the system investigated, litidionite *sensu stricto* is the primary litidionite-group species, followed by calcinaksite and Ti-bearing litidionite. The volcanic silicate glass from the lapilli with litidionite contains up to 3 wt.% of TiO_2 . Partial crystallisation of this glass probably leads to the formation of Ti-bearing minerals such as perovskite, rutile, kamenevite and Ti-bearing litidionite. The latest litidionite crystals to form can also accommodate Pb (up to 4.27 wt.%) and Cl (up to 0.21 wt.%).

The five-coordinated site in litidionite-group minerals can be occupied by Cu^{2+} in litidionite, Fe^{2+} in fenaksite, Mn^{2+} in manaksite and by Ca^{2+} in calcinaksite with 5+1 coordination (Golovachev et al., 1970; Pozas et al., 1975; Khomyakov et al., 1992; Aksenov et al., 2014). All these cations are divalent.

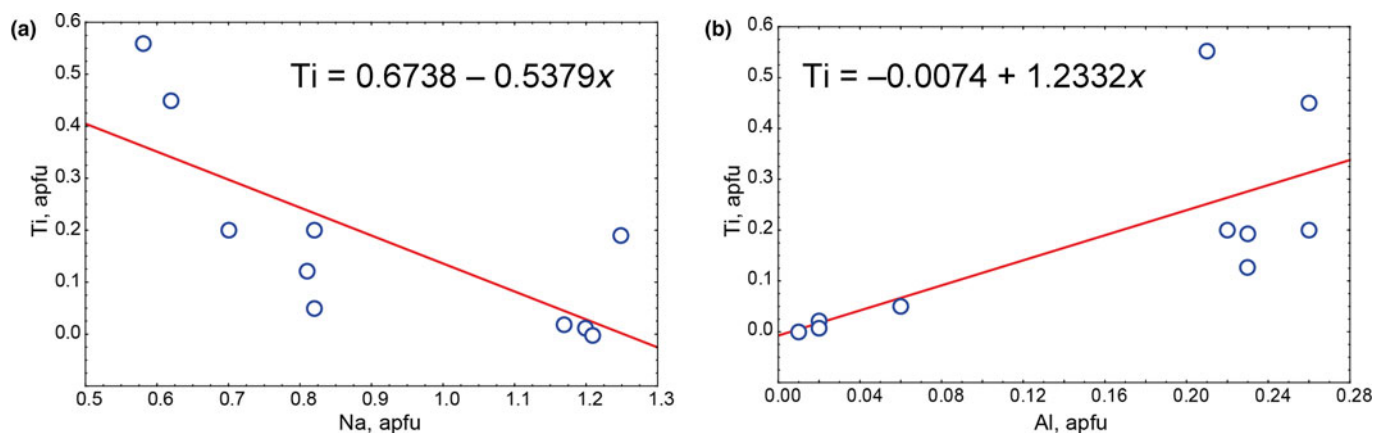


Fig. 8. Relations between the cation contents in litidionite of (a) Ti and Na ($R^2 = 0.55$), and (b) Ti and Al ($R^2 = 0.50$). Sample #17926 E6457.

According to our chemical data, the maximal TiO_2 content is 12.06 wt.% or 0.56 Ti apfu. Incorporation of Ti^{4+} cations is in negative correlation with the Na content (Fig. 8a) and correlates positively with the Al content (Fig. 8b). Incorporation of Ti^{4+} into the litidionite structure can be explained by the complex substitution ${}^{\text{VI}}\text{Ti}^{4+} + {}^{\text{VII-VIII}}\square + {}^{\text{IV}}\text{Al}^{3+} \leftrightarrow {}^{\text{V}}\text{Cu}^{2+} + {}^{\text{VII-VIII}}(\text{Na,K})^+ + {}^{\text{IV}}\text{Si}^{4+}$. The excessive charge in the M site is most likely compensated by the formation of vacancies at the Na or K sites.

The Ti is a charge-dominant component at the M site (Table 1, analysis 5) with a Ti^{4+} charge of 2.24 and sum for Mg^{2+} , Ca^{2+} , Cu^{2+} and Fe^{2+} of 1.12; the observed composition of the M site ($\text{Ti}_{0.56}\text{Mg}_{0.29}\text{Cu}_{0.11}\text{Ca}_{0.10}\text{Fe}_{0.06}$) $_{\Sigma 1.12}$ corresponds to the composition of a new litidionite-group mineral according to the application of the dominant-valency rule (Bosi *et al.*, 2019). However, zones of the Ti-bearing litidionite studied by single-crystal X-ray diffraction correspond to an M site occupancy of ($\text{Ti}_{0.32}\text{Cu}_{0.30}\text{Ca}_{0.29}\text{Fe}_{0.09}$) $_{\Sigma 1.00}$, which does not correspond to the new litidionite mineral composition.

In litidionite-group minerals, the M site is populated by different cations, whereas the rest of structure does not change; the same is observed for the vesuvianite-group minerals, which crystallise under similar temperature conditions (Panikorovskii *et al.*, 2017a, 2017b, 2017c, 2017d). In vesuvianite, the 5-coordinated position demonstrates significant variability (by Fe^{3+} , Fe^{2+} , Mg, Mn^{2+} , Mn^{3+} and Cu^{2+}) accompanied by the change in the polyhedral volume of the Y1 site within 30%. The five-coordinated M site in the litidionite-group minerals can be occupied by Ca^{2+} , Cu^{2+} , Mn^{2+} , Fe^{2+} and Ti^{4+} . The diverse occupancy of the M site (square pyramid in litidionite) is related to the flexibility of the MO_5 -polyhedra, possible population of the additional intra-channel O11 site and the variability of distances between the neighbouring silicate tubes. The M site in the litidionite-group minerals can possess different coordination environments: square-pyramidal (litidionite, manaksite), trigonal prismatic (fenaksite) and octahedral (calcinaksite). The polyhedral volume of the M site may change from 7.06 in litidionite to 16.93 Å³ in calcinaksite. Such a flexibility of coordination and polyhedral volumes results in high chemical capacity and cationic diversity, which allows one to predict possible new litidionite-group species with different occupancies of the M site.

Examples of mineral-inspired materials in materials science are few and include zorite (ETS-4), ivanyukite (GTS, SIV), kamelevite (AM-2, STS) and sitinakite (IONSIV-911, TAM-5, STS, CST) (Oleksiienko *et al.*, 2017). Incorporation of Ti into litidionite with creation of vacancies at the K site makes it possible to

consider this phase as a prospective material for the selective removal of radionuclides from waste aqueous solutions. According to our recent studies, calcination of the ion-exchanged forms of titanosilicates up to 1000°C results in the formation of Synroc-type titanate ceramics.

Conclusions

Active volcanic fumaroles can be considered as natural laboratories with the possibility to study *in situ* the processes of mineral formation, geochemical behaviour and migration of chemical elements (Shchিপalkina *et al.*, 2020b). Even though in Vesuvius ejecta, Ti is a trace element, it can form independent phases (e.g. perovskite, rutile and kamelevite) at the last stages of mineral evolution.

This study demonstrated that the flexibility of the litidionite structure is much stronger than previously thought and involves not only isoivalent substitutions at the M site. The incorporation of Ti into the litidionite structure is accompanied by complex heterovalent substitution by the scheme ${}^{\text{VI}}\text{Ti}^{4+} + {}^{\text{VII-VIII}}\square + {}^{\text{IV}}\text{Al}^{3+} \leftrightarrow {}^{\text{V}}\text{Cu}^{2+} + {}^{\text{VII-VIII}}(\text{Na,K})^+ + {}^{\text{IV}}\text{Si}^{4+}$. Replacing one Cu^{2+} atom by Ti^{4+} at the M site is accompanied by the replacement of Si^{4+} by Al^{3+} at the T site and the formation of a vacancy (\square) at the Na or K sites. We noted significant Ti (up to 0.56 apfu) and Mg (up to 0.34 apfu) amounts that incorporate into the M site, which leads us to assume the possible end-members of the litidionite group, $\text{CuTiK}\square\text{Na}_2\text{Si}_7\text{AlO}_{20}$ ($Z = 1$) or $\text{CuTiK}_2\text{Na}\square\text{Si}_7\text{AlO}_{20}$ ($Z = 1$) and $\text{MgKNaSi}_4\text{O}_{10}$ ($Z = 2$). The chemical diversity at the M site is possible owing to the flexibility of site coordination connected with the variability of distances between neighbouring $[\text{Si}_8\text{O}_{20}]_{\infty}^{8-}$ tubes.

Acknowledgements. This work is dedicated to the memory of Prof. Enrico Franco, who introduced GB to the study of the Somma-Vesuvius minerals. Authors are grateful to the Principal Editor Dr. Stuart Mills and referees Prof. Peter Leverett and two anonymous reviewers for the constructive comments that significantly improved paper quality. R. de Gennaro (DiSTAR, Naples) is thanked for SEM-EDS analyses. The technical support of M. Serracino (IGAG CNR, Rome) with WDS analyses (IGAG-CNR, Rome) is greatly appreciated. The research is supported by the Russian Foundation for Basic Research, grant 18-29-12039 and by the Kola Science Center of Russian Academy of Sciences (AAAA-A19-119111190038-5). X-ray diffraction studies were performed at the XRD Research Resource Centre and Geomodel of St. Petersburg State University. G. Balassone also benefited from the fund # "Ricerca Dipartimentale 2020" granted by the University of Napoli Federico II (Italy).

Supplementary material. To view supplementary material for this article, please visit <https://doi.org/10.1180/mgm.2022.1>

References

- Agilent Technologies (2014) *CrysAlis CCD and CrysAlis RED*. Oxford Diffraction Ltd, Yarnton, Oxfordshire, UK.
- Aksenov S.M., Rastsvetaeva R.K., Chukanov N.V. and Kolitsch U. (2014) Structure of calcinaksite $\text{KNa}[\text{Ca}(\text{H}_2\text{O})][\text{Si}_4\text{O}_{10}]$, the first hydrous member of the litidionite group of silicates with $[\text{Si}_8\text{O}_{20}]^{8-}$ tubes. *Acta Crystallographica*, **B70**, 768–775.
- Arrighi S., Principe C. and Rosi M. (2001) Violent strombolian and subplinian eruptions at Vesuvius during post-1631 activity. *Bulletin of Volcanology*, **63**, 126–150.
- Avanzinelli R., Cioni R., Conticelli S., Giordano G., Isaia R., Mattei M., Melluso L. and Sulpizio R. (2017) The Vesuvius and the other Volcanoes of Central Italy. *Geological Field Trips*, **9** (1.1), <http://www.isprambiente.gov.it/it/publicazioni/periodici-tecnici/geological-field-trips> [accessed on 5 January 2021].
- Balassone G., Franco E., Mattia C.A. and Puliti R. (2004) Indialite in xenolithic rocks from Somma–Vesuvius volcano (Southern Italy): crystal chemistry and petrogenetic features. *American Mineralogist*, **89**, 1–6.
- Balassone G., Petti C., Mondillo N., Panikorovskii T.L., de Gennaro R., Cappelletti P., Altomare A., Corriero N., Cangiano M. and D’orazio L. (2019) Copper minerals at vesuvius volcano (Southern Italy): A mineralogical review. *Minerals*, **9**, 730.
- Balić-Zunić T., Garavelli A., Jakobsson S.P., Jonasson K., Katerinopoulos A., Kyriakopoulos K. and Acquafredda P. (2016) Fumarolic minerals: An overview of active European volcanoes. Pp. 267–322 in: *Updates in Volcanology – From Volcano Modelling to Volcano Geology* (K. Nemeth, editor). InTech Open Access Publishers, London, UK.
- Baur W.H. (1974) The geometry of polyhedral distortions. Predictive relationships for the phosphate group. *Acta Crystallographica*, **B30**, 1195–1215.
- Bosi F., Hatert F., Hälenius U., Pasero M., Miyawaki R. and Mills S.J. (2019) On the application of the IMA–CNMNC dominant-valency rule to complex mineral compositions. *Mineralogical Magazine*, **83**, 627–632.
- Brandão P., Rocha J., Reis M.S., dos Santos A.M. and Jin R. (2009) Magnetic properties of compounds. *Journal of Solid State Chemistry*, **182**, 253–258.
- Castor S.B. and Ferdock G.C. (2003) *Minerals of Nevada*. Nevada Bureau of Mines and Geology, Special Publication, 31, Nevada, USA, 560 pp.
- Celestian A.J., Powers M. and Rader S. (2013) In situ Raman spectroscopic study of transient polyhedral distortions during cesium ion exchange into sitinakite. *American Mineralogist*, **98**, 1153–1161.
- Chukanov N.V., Aksenov S.M., Rastsvetaeva R.K., Blass G., Varlamov D.A., Pekov I.V., Belakovskiy D.I. and Gurzhiy V.V. (2015) Calcinaksite, $\text{KNaCa}(\text{Si}_4\text{O}_{10})\cdot\text{H}_2\text{O}$, a new mineral from the Eifel volcanic area, Germany. *Mineralogy and Petrology*, **109**, 397–404.
- Cioni R., Santacroce R. and Sbrana A. (1999) Pyroclastic deposits as a guide for reconstructing the multi-stage evolution of the Somma–Vesuvius caldera. *Bulletin of Volcanology*, **60**, 207–222.
- Cioni R., Bertagnini A., Santacroce R. and Andronico D. (2008) Explosive activity and eruption scenarios at Somma–Vesuvius (Italy): Towards a new classification scheme. *Journal of Volcanology and Geothermal Research*, **178**, 331–346.
- Di Renzo V., Di Vito M. A., Arienzo I., Carandente A., Civetta L., D’antonio M. and Tonarini S. (2007) Magmatic history of Somma–Vesuvius on the basis of new geochemical and isotopic data from a deep borehole (Camaldoli della Torre). *Journal of Petrology*, **48**, 753–784.
- Dolivo-Dobrovolsky D.D. (2016) MINAL, free software. Saint-Petersburg [Accessed from <http://www.dimadd.ru>].
- Filippi M., Doušová B. and Machovič V. (2007) Mineralogical speciation of arsenic in soils above the Mokrsko-west gold deposit, Czech Republic. *Geoderma*, **139**, 154–170.
- Golovachev V.P., Drozdov Y.N., Kuz’min E.A. and Belov N.V. (1970) The crystal structure of fenaksite, $\text{NaKFeSi}_4\text{O}_{10}$. *Doklady Akademii Nauk SSSR*, **194**, 818–820 [in Russian].
- Khomaykov A.P., Kurova T.A. and Nchelyustov G.N. (1992) Manaksite $\text{NaKMnSi}_4\text{O}_{10}$: a new mineral. *Zapiski RMO*, **121**, 112–114.
- Kornev A.N., Maksimov B.A., Lider V.V., Ilyukhin V.V. and Belov N.V. (1972) Crystal structure of $\text{Na}_2\text{CuSi}_4\text{O}_{10}$. *Soviet Physics Doklady*, **17**, 735–737.
- Lafuente B., Downs R.T., Yang H. and Stone N. (2015) The power of databases: the RRUFF project. Pp 1–30 in: *Highlights in Mineralogical Crystallography* (T. Armbruster and R.M. Danisi, editors). De Gruyter, Berlin, Germany.
- Momma K. and Izumi F. (2011) VESTA 3 for three-dimensional visualization of crystal, volumetric and morphology data. *Journal of Applied Crystallography*, **44**, 1272–1276.
- Oleksienko O., Wolkersdorfer C. and Sillanpää M. (2017) Titanosilicates in cation adsorption and cation exchange – A review. *Chemical Engineering Journal*, **317**, 570–585.
- Pakhomovsky Y.A., Panikorovskii T.L., Yakovenchuk V.N., Ivanyuk G.Y., Mikhailova J.A., Krivovichev S. V., Bocharov V.N. and Kalashnikov A.O. (2018) Selivanovite, $\text{NaTi}_3(\text{Ti},\text{Na},\text{Fe},\text{Mn})_4[(\text{Si}_2\text{O}_7)_2\text{O}_4(\text{OH},\text{H}_2\text{O})_4]\cdot n\text{H}_2\text{O}$, a new rock-forming mineral from the eudialyte-rich malignite of the Lovozero alkaline massif (Kola Peninsula, Russia). *European Journal of Mineralogy*, **30**, 525–535.
- Panikorovskii T.L., Chukanov N.V., Aksenov S.M., Mazur A.S., Avdontseva E.Y., Shilovskikh V.V. and Krivovichev S.V. (2017a) Alumovesuvianite, $\text{Ca}_{19}\text{Al}(\text{Al},\text{Mg})_{12}\text{Si}_{18}\text{O}_{69}(\text{OH})_9$, a new vesuvianite-group member from the Jeffrey mine, Asbestos, Estrie region, Québec, Canada. *Mineralogy and Petrology*, **111**, 833–842.
- Panikorovskii T.L., Chukanov N.V., Rusakov V.S., Shilovskikh V.V., Mazur A.S., Balassone G., Ivanyuk G.Y. and Krivovichev S.V. (2017b) Vesuvianite from the Somma–Vesuvius Complex: New Data and Revised Formula. *Minerals*, **7**, 248.
- Panikorovskii T.L., Shilovskikh V.V., Avdontseva E.Y., Zolotarev A.A., Karpenko V.Y., Mazur A.S., Yakovenchuk V.N., Bazai A.V., Krivovichev S.V. and Pekov I.V. (2017c) Magnesiovesuvianite, $\text{Ca}_{19}\text{Mg}(\text{Al},\text{Mg})_{12}\text{Si}_{18}\text{O}_{69}(\text{OH})_9$, a new vesuvianite-group mineral. *Journal of Geosciences*, **62**, 25–36.
- Panikorovskii T.L., Shilovskikh V.V., Avdontseva E.Y., Zolotarev A.A., Pekov I.V., Britvin S.N., Hälenius U. and Krivovichev S.V. (2017d) Cyprine, $\text{Ca}_{19}\text{Cu}^{2+}(\text{Al},\text{Mg},\text{Mn})_{12}\text{Si}_{18}\text{O}_{69}(\text{OH})_9$, a new vesuvianite-group mineral from the Wessels mine, South Africa. *European Journal of Mineralogy*, **29**, 295–306.
- Pekov I.V., Sandalov F.D., Koshlyakova N.N., Viganina M.F., Polekhovskiy Y.S., Britvin S.N., Sidorov E.G. and Turchkova A.G. (2018) Copper in natural oxide spinels: the new mineral thermaerogenite CuAl_2O_4 , cuprospinel and Cu-enriched varieties of other spinel-group members from fumaroles of the Tolbachik Volcano, Kamchatka, Russia. *Minerals*, **8**, 498, <https://doi.org/10.3390/min8110498>.
- Pekov I.V., Zubkova N.V., Yapaskurt V.O., Belakovskiy D.I., Lykova I.S., Britvin S.N., Turchkova A.G. and Pushcharovskiy D.Y. (2019) Kamenevite, $\text{K}_2\text{TiSi}_3\text{O}_9\cdot\text{H}_2\text{O}$, a new mineral with microporous titanosilicate framework from the Khibiny alkaline complex, Kola peninsula, Russia. *European Journal of Mineralogy*, **31**, 557–564.
- Pouchou J.L. and Pichoir F. (1991) Quantitative analysis of homogeneous or stratified microvolumes applying the model “PAP”. Pp. 31–76 in: *Electron Probe Quantitation* (Heinrich K. and Newbury D., editors). Plenum Press, New York.
- Pozas J.M., Rossi G. and Tazzoli V. (1975) Re-examination and crystal structure analysis of litidionite. *American Mineralogist*, **60**, 471–474.
- Rozhdestvenskaya I.V., Bannova I.I., Nikishova L.V. and Soboleva T.V. (2004) The crystal structure of fenaksite $\text{K}_2\text{Na}_2\text{Fe}_2\text{Si}_8\text{O}_{20}$. *Doklady of the Russian Academy of Sciences*, **398**, 1029–1033.
- Scacchi E. (1880) Lapilli azzurri del Vesuvio. *Atti della Regia Accademia delle Scienze Fisiche e Matematiche di Napoli*, **19**, 175–179.
- Scacchi A. (1881) Nuovi sublimati del cratere vesuviano trovati nel mese di ottobre del 1880 (Memoria 1880). *Atti della Reale Accademia delle Scienze Fisiche e Matematiche di Napoli*, Serie I, **9**, 1–10.
- Shchepalkina N.V., Pekov I.V., Britvin S.N., Koshlyakova N.N., Viganina M.F. and Sidorov E.G. (2019) A new mineral ferrisanidine, $\text{K}[\text{Fe}^{3+}\text{Si}_3\text{O}_8]$, the first natural feldspar with species-defining iron. *Minerals*, **9**, 770.
- Shchepalkina N.V., Pekov I. V., Britvin S.N., Koshlyakova N.N. and Sidorov E.G. (2020a) Arsenic and phosphorus in feldspar framework: sanidine–

- filatovite solid solution series from fumarolic exhalations of the Tolbachik volcano, Kamchatka, Russia. *Physics and Chemistry of Minerals*, **47**, 1–15.
- Shchipalkina N.V., Pekov I.V., Koshlyakova N.N., Britvin S.N., Zubkova N.V., Varlamov D.A. and Sidorov E.G. (2020b) Unusual silicate mineralization in fumarolic sublimates of the Tolbachik volcano, Kamchatka, Russia – Part 1: Neso-, cyclo-, ino- and phyllosilicates. *European Journal of Mineralogy*, **32**, 101–119.
- Shchipalkina N. V., Pekov I. V., Koshlyakova N.N., Britvin S.N., Zubkova N. V., Varlamov D.A. and Sidorov E.G. (2020c) Unusual silicate mineralization in fumarolic sublimates of the Tolbachik volcano, Kamchatka, Russia. Part 2: Tectosilicates. *European Journal of Mineralogy*, **32**, 121–136.
- Sheldrick G.M. (2015) Crystal structure refinement with SHELXL. *Acta Crystallographica*, **C71**, 3–8.
- StatSoft Inc. (2008) *Statistica* 8. StatSoft. Inc., Tulsa, OK74104, USA.
- Yakovenchuk V., Pakhomovsky Y., Panikorovskii T.L., Zolotarev A., Mikhailova J., Bocharo V., Krivovichev S. and Ivanyuk G. (2019) Chirvinskyite, $(\text{Na,Ca})_{13}(\text{Fe,Mn},\square)_2(\text{Ti,Nb})_2(\text{Zr,Ti})_3(\text{Si}_2\text{O}_7)_4(\text{OH,O,F})_{12}$, a new mineral with a modular wallpaper structure, from the Khibiny Alkaline Massif (Kola Peninsula, Russia). *Minerals*, **9**, 219.
- Zambonini F. (1910) Mineralogia Vesuviana. *Atti Real Accademia Scienze Fisiche e Naturali di Napoli*, Series 2, **14**, 368 pp.
- Zambonini F. (1935) Mineralogia Vesuviana. *SIEM Napoli*, XIII, 468 pp.